# JOINT EFFECTS OF DYNAMIC TIME SLOT SCHEDULING SCHEMES AND SOFT HANDOFF ON THE PERFORMANCE OF TDD DS-CDMA SYSTEMS WITH 2D RAKE RECEIVERS

**Roger Pierre Fabris Hoefel and Celso de Almeida**

**Abstract** – In this paper, we derive analytical expressions to assess the performance of Time Division Duplexing (TDD) Direct Sequence-Code Division Multiple Access (DS-CDMA) systems with coherent bi-dimensional (2D) Rake receivers. Considering either hexagonal macrocellular and microcellular cross-shaped networks, we propose and evaluate different approaches to model the effects of the intercellular multiple access interference (MAI) on the performance of DS-CDMA systems with 2D Rake receivers. These results are then used on the performance comparison between coherent and optimum 2D Rake receivers. It is shown that soft handoff allows gains of 2 dB in the Signal-to-Interference-plus-Noise-Ratio (SINR) at the 2D Rake receiver output. Simulation results, ratified by theoretical upper bounds, show that the dynamic time slot allocation schemes allow considerable increase of the SINR at the receiver output with a concomitant improvement on the throughput.

**Keywords:** CDMA, TDD, 2D Rake, adaptive antennas, soft handoff, dynamic time slot scheduling, MAC protocols.

**Resumo** – Neste artigo apresenta-se expressões analíticas para analisar o desempenho de sistemas TDD DS-CDMA (do inglês Time Division Duplexing Direct Sequence-Code Division Multiple Access) com receptores do tipo Rake bidimensional. Considerando-se redes macro e micro celular, propõe-se e avalia-se distintos métodos para modelar os efeitos da interferência externa no desempenho de sistemas DS-CDMA com receptores Rake bidimensional. A partir destes resultados, realiza-se uma comparação entre o desempenho dos receptores Rake coerentes e os receptores Rake com resposta ótima. Constata-se ainda que a técnica de *soft handoff* propicia ganhos de 2 decibéis na Razão-Sinal-Interferência (RSI) observada na saída do receptor Rake bidimensional. Resultados de simulações, ratificados por limitantes teóricos superiores, mostram que esquemas de escalonamento de canal permitem um aumento da RSI na saída do receptor bem como uma maior eficiência na utilização do canal.

**Palavras chave:** CDMA, TDD, receptor RAKE bidimensional, antenas adaptativas, escalonamento dinâmico de canal, protocolos para acesso ao meio.

Roger Pierre Fabris Hoefel is at Department of Telecommunications Engineering of the University La Salle (UNILASALLE) - Canoas - RS – Brazil – 92.010-000. Celso de Almeida is at State University of Campinas (UNICAMP). E-mail: roger@lasalle.tche.br.

## 1 INTRODUCTION

Considering a multitude of parameters, it has been concluded that the time variant and irregular spatial-temporal channel characteristics have a strong influence on the performance of TDD DS-CDMA systems with 2D RAKE receivers [1]. In this paper, it is shown that dynamic time slot allocation algorithms substantially improve the uplink performance of TDD DS-CDMA systems with wavefield transceivers. In order to accomplish the above mentioned objective, this paper has been organized as follows. A description of the 2D Rake receiver is presented in Section 2. Analytical expressions to estimate the performance of the coherent 2D Rake receiver are developed in Section 3. A brief description of a network simulator is done in Section 4. A comparison between analytical and simulation results is carried out in Section 5. The effects of soft handoff and dynamic time slot scheduling on the system performance are investigated in Section 6 and 7, respectively. Finally, some final remarks are done in Section 8.

## 2 2D RAKE RECEIVER

The 2D Rake receiver, constituted of an array of M antennas and P taps per antenna, reduces interference by means of spatial and temporal processing in order to produce an improved decision variable to the detection circuit. A description of 2D Rake receiver can be found in [2, pp. 81]. At this section, it is presented the steps to numerically estimate the SINR at the 2D Rake receiver output.

Assuming a chip and phase synchronous system, the SINR for the *k-th* user in a interference limited coherent binary phase shift keying (BPSK) DS-CDMA system can be evaluated by [3, pp. 40]:

$$SINR_k = \frac{G_p \mathbf{W}_k^H \mathbf{R}_{s,k} \mathbf{W}_k}{\mathbf{W}_k^H \mathbf{R}_{u,k} \mathbf{W}_k}, \qquad (1)$$

where $G_p$ is the processing gain; $\mathbf{W}_k$ is a column vector that contains the MP coefficients of the 2D Rake receiver for the *k-th* target user; $\mathbf{R}_{s,k}$ is the desired signal covariance matrix, $\mathbf{R}_{u,k}$ is the MAI plus noise covariance matrix observed by the *k-th* user; and $(.)^H$ represents the Hermitian operator.

Assuming a frequency selective fading channel with inbound diversity L and negligible intersymbolic interference ($L \ll G_p$), then the *k-th* user's M by L channel matrix can be stated as:

$$\mathbf{H}_k = \sqrt{P_k}\,[\mathbf{h}_{k,0}\ \mathbf{h}_{k,1} \cdots \mathbf{h}_{k,L-1}], \qquad (2)$$

where $\mathbf{h}_{k,l}$ is the M column vector that models the arrival at the antenna array of *l-th* multipath of the *k-th* user. $P_{k,l}$

models the average power per antenna received due to the *k-th* terminal. It is equal to one when the MS is controlled by the target BS, and $P_k$, as explained at Section 4, is a function of, among other parameters, the user spatial location, path loss and log-normal shadowing when this MS contributes with external MAI to the target cell.

For an antenna array (AA) with M correlated antennas (i.e. the number of spatial diversity branches $M_D$ is equal to 1), the steering vector is given by:

$$\mathbf{h}_{k,l} = \alpha_{k,l}[e^{j\beta_{k,0,l}} \; e^{j\beta_{k,1,l}} \cdots e^{j\beta_{k,M-1,l}}]^T. \quad (3)$$

where $\alpha_{k,l}$ is a complex random variable (RV) that models the channel gain for the *l–th path* of *k-th* user.

If it is assumed an array with M correlated antennas, then the relative phase at the *m-th* element for a linear equally spaced (LES) is given by [3, pp. 16]:

$$\beta_{k,m,l} = m\frac{2\pi}{\lambda} d\sin(\theta_{k,l}), \quad (4)$$

where $d$ is the spacing between the isotropic array elements, $\lambda$ is the wavelength of frequency carrier, and $\theta_{k,l}$ is the Direction-of-Arrival (DOA) at the azimuth for the *l–th* path of the *k-th* user.

For a circular equally spaced (CES) array with M correlated antennas, the relative phase at the *m-th* element with respect to the center of the circular array of radius R is given by [3, pp. 17]:

$$\beta_{k,l,m} = -\frac{2\pi}{\lambda} R\cos\left(\theta_{k,l} - \frac{2m\pi}{M}\right). \quad (5)$$

If the multipath fading is uncorrelated in all antenna elements (i.e. $M_D$=M), then the spatial temporal signature for both topologies (i.e. LES and CES arrays) is given by:

$$\mathbf{h}_{k,l} = [\alpha_{k,l,0} \cdots \alpha_{k,l,M-1}]^T, \quad (6)$$

where $\alpha_{k,l,m}$ is a complex RV that models the channel gain for k-th user at the *l–th* path at the *m-th* antenna element. It can be emphasized that in (3) the channel complex gain is equal in each antenna element, i.e. $\alpha_{k,l}=\alpha_{k,l,m}$ (m=1,...,M), due to the spatial correlation assumption. The second moment of channel gain per antenna is normalized, i.e.

$$\sum_{l=0}^{L-1} E\left[\left|\alpha_{k,l,m}\right|^2\right] = 1 \quad for\ m = 0, \cdots, M-1. \quad (7)$$

Noticing that the solution that minimizes the mean square error (MSE) of chip sequence also minimizes the MSE of symbol sequence estimation [2, pp. 89], then the spatial covariance matrix (dimension MP by MP) of interference-plus-noise at the target cell can be stated as:

$$\mathbf{R} = \sum_{j=1}^{KN_{BS}} H_j H_j^H + \sigma_n^2 \mathbf{I}_{MP}, \quad (8)$$

where K is the number of MSs physically located in each of one of $N_{BS}$ hexagonal BSs, and the Additive White Gaussian Noise (AWGN) power in a bandwidth W is $2\sigma_n^2 W$, where $N_o=2\sigma_n^2$ is the noise one-side power spectral density. $\mathbf{I}_{MP}$ is the identity matrix of order MP. The multipath channel response is a matrix of dimension MP by P+L-1:

$$H_k = \begin{vmatrix} \mathbf{H}_k & \mathbf{0} & \cdots & \mathbf{0} \\ \mathbf{0} & \mathbf{H}_k & \cdots & \vdots \\ \vdots & \vdots & \ddots & \mathbf{0} \\ \mathbf{0} & \cdots & \mathbf{0} & \mathbf{H}_k \end{vmatrix}, \quad (9)$$

where $\mathbf{0}$ is a M×1 all-zero vector [2, pp. 87]. In derivation of (9), it was assumed, in agreement with the quasi-synchronous assumption, a finite impulsive response (FIR) multipath channel with L taps and whose delay between each multipath was set to one chip period.

The cross-correlation between the *k-th* user's symbol sequence and the whole received signal is given by:

$$\mathbf{p}_k = \mathbf{H}_k \mathbf{e}_P = \mathbf{H}_k^{(P)}. \quad (10)$$

where $\mathbf{e}_P$ is a column vector of dimension (P+L-1) with ones at the *P-th* position and zeros elsewhere, and $\mathbf{H}_k^{(P)}$ indicates the *P-th* column of $\mathbf{H}_k$.

The signal covariance matrix for the *k-th* target user, with dimension MP by MP, is given by:

$$\mathbf{R}_{s,k} = \mathbf{p}_k \mathbf{p}_k^H. \quad (11)$$

Therefore, the MAI plus noise covariance matrix observed by the k-th user is given by:

$$\mathbf{R}_{u,k} = \mathbf{R} - \mathbf{R}_{s,k}. \quad (12)$$

Using the Wiener-Kolmogorov theory [4, pp. 194], the $\mathbf{W}_k$ that minimizes the MSE at 2D Rake receiver output is given by:

$$\mathbf{W}_{ot,k} = \mathbf{R}^{-1}\mathbf{p}_k. \quad (13)$$

Using Woodbury's identity (or matrix inversion lemma [3, pp. 39]) to $\mathbf{R}^{-1}$ ($\mathbf{R}$ is given by Eq. 8), then the maximum SINR solution for the *k-th* user can be stated as:

$$\mathbf{W}_k = \beta \mathbf{R}_{\mathbf{U}_k}^{-1} \mathbf{p}_k, \quad (14)$$

where $\beta$ is a scale constant which does not affect the SINR, as it equally applies to all signals.

Using (14) in (1), the SINR can be rewritten as:

$$SINR = G_p \, \mathbf{p}_k^H \mathbf{R}_{\mathbf{U}_k}^{-1} \mathbf{p}_k. \quad (15)$$

Finally, it has been noticed that the Liu's definition for the SINR (where MMSE is the minimum MSE at the 2D Rake receiver output [2, pp. 89-93]), i.e.

$$SINR = \frac{1}{MMSE} = 1 + G_p \, \mathbf{p}_k^H \mathbf{R}_{\mathbf{U}_k}^{-1} \mathbf{p}_k, \quad (16)$$

is only valid if $G_p \mathbf{p}_k^H \mathbf{R}_{\mathbf{U}_k}^{-1} \mathbf{p}_k >> 1$.

## 3 COHERENT 2D RAKE RECEIVER

In this section, it is assumed the following: *(i)* a receiver with M antennas and P taps per antenna whose response is obtained by the Maximum Ratio Combining (MRC) or coherent solution; *(ii)* the MAI is modeled as a flat power spectrum density and all received signals have the same average power; *(iii)* the fading is independent in all antennas (i.e. $M_D$=M). As the trace of a scalar is a scalar itself, then the SINR (Eq. 1) can be rewritten as:

$$SINR_k = \frac{G_p \mathbf{W}_k^H \mathbf{R}_{s,k} \mathbf{W}_k}{E\left[\mathbf{W}_k^H \mathbf{R}_{u,k} \mathbf{W}_k\right]}, \quad (17)$$

where tr($\mathbf{A}$) denotes the trace of matrix $\mathbf{A}$, and $\mathbf{W}_k = \mathbf{p}_k^*$ due to MRC assumption (* denotes the complex conjugate). Taking into account that the received signals at the antenna array are spatially and temporally white and that it is assumed that the receiver temporal diversity is matched

with the channel inbound diversity (i.e. P=L), then the outcomes are as follows:

$$\mathbf{R}_{s,k} = M\ \mathbf{I}_{MP}, \tag{18}$$

$$\mathbf{R}_{u,k} \cong K(1+f)\mathbf{I}_{MP} + \sigma_n^2 \mathbf{I}_{MP}, \tag{19}$$

where f is the relative other-cell interference factor [5, pp. 189]. Finally,

$$SINR_k = \frac{G_p tr(\mathbf{p}_k \mathbf{p}_k^H \mathbf{R}_{s,k})}{E\left[tr(\mathbf{p}_k \mathbf{p}_k^H \mathbf{R}_{u,k})\right]} \approx \frac{G_p M\left(\sum_{m=1}^{MP} \left|\alpha_{k,m}\right|^2\right)}{MP\frac{1}{P}K(1+f)}, \tag{20}$$

where the AWGN has been neglected due to interference limited assumption and the factor 1/P=1/L in the denominator comes from (7). It has also been used that the trace of matrix product **AB** equals the trace of matrix *product* ***BA***.

If the magnitude of multipath fading is supposed to be a Nakagami-m RV, it can be verified that the SNIR probability density function (PDF) at the output of the MRC 2D Rake receiver is of Gamma kind with shape parameter β equals to MPm [6]:

$$p(x) = \begin{cases} \frac{1}{\Gamma(\beta)}\left(\frac{m}{\overline{SINR}}\right)^{\beta}(x)^{\beta-1}exp\left(-\frac{mx}{\overline{SINR}}\right) & if\ x>0,\ m\geq 0.5, \\ 0 & elsewhere \end{cases} \tag{21}$$

where Γ(z) is the gamma function, and

$$\overline{SINR} = \frac{G_p(1/P)}{K(1+f)}. \tag{22}$$

Observing that: *(i)* (22) models the SINR at each one of the MP fingers of the MRC receiver (it is assumed that P=L); *(ii)* the spatial-temporal diversity gain is implicated in the shape parameter β=MPm; *(iii)* for a receiver with just one antenna and one finger, then the SINR at the receiver output is also Gamma distributed, but with the shape parameter β in (21) equals to *m* (the Nakagami-m fading figure). Finally, it can remarked that the Gamma RV degenerates in an impulse function when β→∞.

The jargon *pole point* or *pole capacity* is used to designate the capacity obtained with perfect power control assumption and neglectable AWGN assumptions, but which serves as a useful reference point for network planners. Evidently, the 2D RAKE receiver reduces to an antenna array (AA) receiver if the number of filter taps per antenna, P, is set to one. Therefore, the spatial signature for an LES AA receiver over an AWGN channel is given by:

$$\mathbf{h}_k = \sqrt{P_k}\left[1\ e^{j\pi sin\theta_k} \cdots e^{j(M-1)\pi sin\theta_k}\right]^T. \tag{23}$$

Therefore, a coherent combining receiver has a normalized response given by:

$$\mathbf{W}_k^H = \sqrt{P_k}\left[1\ e^{-j\pi sin\theta_k} \cdots e^{-j(M-1)\pi sin\theta_k}\right] / \left(\left\|\mathbf{h}(\theta_k)\right\|\right), \tag{24}$$

where $\|\mathbf{h}_k\|$ is the Euclidian norm of the steering vector $\mathbf{h}_k$.

Modeling the MAI as a flat power spectrum, then the normalized MAI interference at AA output can be stated as:

$$\frac{I}{K(1+f)} = \frac{1}{M}\sum_{m=0}^{M-1}\sum_{n=0}^{M-1} E\left[e^{-j\pi(n-m)sin\theta}\right] E\left[e^{j\pi(n-m)sin\phi}\right]. \tag{25}$$

where θ and φ are RVs that model the DOA at the azimuth direction. So, for pole capacity calculations, the average SINR at AA receiver output is given by:

$$\overline{SINR} \approx G_p \frac{M^2}{K(1+f)\sum_{m=0}^{M-1}\sum_{n=0}^{M-1} E\left[e^{-j\pi(n-m)sin\theta}\right] E\left[e^{j\pi(n-m)sin\phi}\right]}. \tag{26}$$

## 4 MICROCELLULAR AND MACROCELLULAR NETWORKS

The main characteristics of the system level simulator with full interactivity between all cells are [7, pp. 185; 344]:

- The network consists of homogenous hexagonal macrocells with 19 BSs or cross-shaped microcells with 25 BSs. It is assumed X=200m and W=50 m (see Fig. 1)
- The MSs are uniformly distributed over the cells.
- The long-term paths loss for line-of-sight (LOS) paths is given by:

$$L_{k,n} = \begin{cases} \frac{10^{\zeta_{k,n}/10}}{r_{k,n}^2}, & for\ r_{k,n} \leq X_b \\ \frac{10^{\zeta_{k,n}/10}}{r_{k,n}^{\Gamma}}, & for\ r_{k,n} > X_b \end{cases}, \tag{27}$$

where $r_{k,n}$ and $\zeta_{k,n}$ denote the distance and the lognormal shadowing, respectively, between the *k-th* MS and the *n-th* BS; Γ is the path loss exponent when $r_{k,n}$ is greater than the distance from the BS antenna to where the curve changes its gradient (i.e. $X_b$). It is observed that the path loss is set to 2 for $r_{k,n}<X_b$. The lognormal shadowing is a Gaussian RV in decibels (dB) with zero mean and standard deviation of $\sigma_{sh}$ dB. Its range is between the open range $-4\sigma_{sh} < \zeta_{k,n} < 2\sigma_{sh}$. For out-of-signal (OOS) path, there is an additional loss $L_{OOS}=20\ dB$ when the MS turns a corner. It is assumed $X_b=0\ m$ and $L_{OOS}=0\ dB$ in the macrocellular hexagonal network.

- The slow power control (PC) dynamics is abstracted in the sense that the average power transmitted by the MSs is the minimum average power to arrive with a unitary average power at each antenna of the minimum loss BS participating in the soft handoff, i.e.

$$P_{tx,k} = min\left(\frac{1}{L_{k,1}}, \frac{1}{L_{k,2}}, \cdots, \frac{1}{L_{k,N_{BS}}}\right). \tag{28}$$

Therefore, the average power received at the target cell due the *k-th* MS is given by:

$$P_k = \frac{P_{tx,k}}{L_{k,1}}. \tag{29}$$

It is emphasized again that $P_k=1$ when the *k-th* MS is controlled by the target cell, i.e. the slow power loop compensates perfectly the attenuation due to the assumed log-linear long-term propagation model (see 2).

- The DOA of each discrete multipath are uniformly $[\bar{\theta}_k - 5^\circ, \bar{\theta}_k + 5^\circ]$ distributed. The mean DOA $\bar{\theta}_k$ is uniformly distributed in each sector (i.e. between $-60^0$ and $+60^0$ in sector 0 and so forth) in macrocellular networks. For microcells the DOA is assumed to be a Gaussian RV with standard deviation of $10^0$ and whose the first moment in South, East, North and West directions are set to $0^0$, $90^0$, $180^0$, $270^0$, respectively.
- In hexagonal topology it is used a LES array at each sector whose elements are separated by half-wavelength of frequency carrier (i.e. d=λ/2 in 4) to avoid grating lobes.
- It is used circular arrays in the cross-shaped microcells to avoid the phase ambiguity that occurs in the LES arrays [3, pp. 16].

Therefore, it is not considered sectorization in the Manhattan cross-shaped microcellular environment.

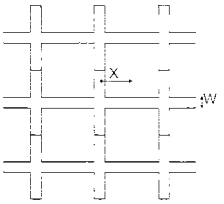


**Figure 1.** Manhattan cross-shaped microcellular network.

## 5 SIMULATION VERSUS ANALYTICAL RESULTS

In this section, the Signal-to-Noise Ratio (SNR) has been set to 100 dB, i.e. interference limited system has been considered. In figures 1 to 3, it is assumed an equal strength (ES) Rayleigh frequency selective fading channel with 3 taps, i.e. L=3.

As a direct consequence of the law of large numbers, Fig. 2 shows that the similitude between analytical and simulation results increases with the channel load.

Besides pointing out the larger effects of spatial diversity on the system performance, Fig. 3 also ratifies the excellent agreement between simulation and analytical results.

Theoretically, it is expected that the intercellular MAI reduce the capability of the optimum 2D RAKE receiver in canceling the interference. Consistently, Fig. 4 shows that the performance gain of the optimum 2D Rake receiver in relation to the MRC 2D Rake receiver diminishes considerably when the intercellular MAI is taken into account. The other cell interference factor f was set to 0.6 to estimate the analytical response when it is assumed a macrocellular cellular system 19 BSs .

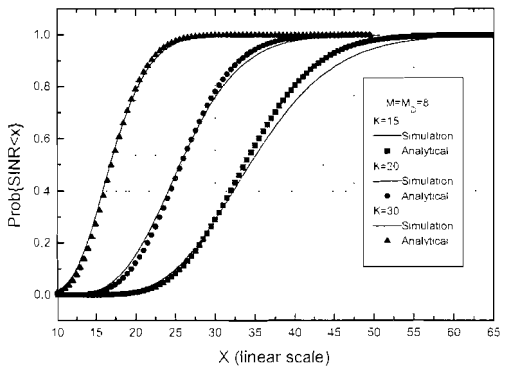


**Figure 2.** Comparison, parameterized by the channel load K, between analytical and simulation results for the MRC 2D Rake receiver. $N_{BS}$=1; $G_p$=64; L=P=3.

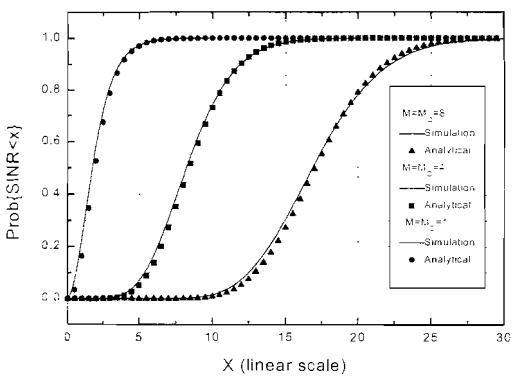


**Figure 3.** Comparison, parameterized by the number of antennas M, between analytical and simulation results for the MRC 2D Rake receiver. $N_{BS}$=1; K=30; $G_p$=64; L=P=3.

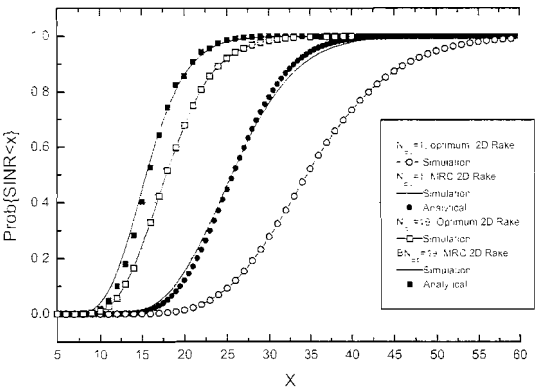


**Figure 4.** Effects of intercell MAI on the performance of the optimum 2D Rake receiver and MRC 2D Rake receiver. $M=M_D$=8; L=P=3; K=20; $G_p$=64; $\Gamma$=4, $\sigma_{sh}$=8 dB.

It is well-known that the Nakagami-m RV reduces to a Rayleigh and exponential negative distribution when the fading figure m is set to 1 and 0.5, respectively. The Nakagami-m RV can also model a Ricean fading with factor $K_{rice}$ if m is set to $(1+K_{rice})^2/(1+2K_{rice})$ [8, pp.43]. Fig. 5 shows that spatial and temporal processing of 2D Rake receiver reduces the effects of fading figure m on the system performance. This figure also shows that the performance of the MRC 2D Rake receiver gets closer to the performance obtained with the optimum 2D Rake receiver when the channel load increases.

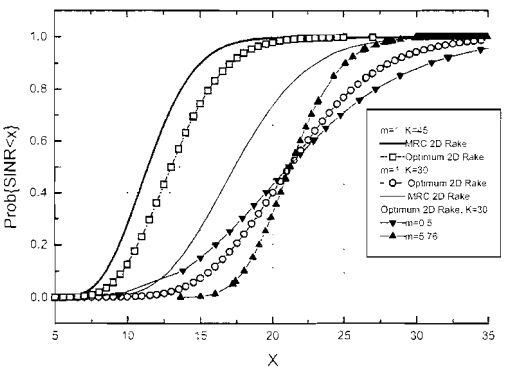


**Figure 5.** Effects of channel load and Nakagami's fading figure on the system performance. $N_{BS}$=1; $G_p$=64; $M=M_D$=8; L=P=3.

For uniformly distributed DOA, Tab. 1a shows: *(i)* a good agreement between numerical (equations 25 and 26) and simulation results; *(ii)* a sensible reduction of system performance in hot spot scenarios (i.e. reduction of DOA spread). Analyzing Tab. 1b it can be infered the following: *(i)* the performance gain due to optimum SINR solution (Eq. 14) reduces considerably when the AA becomes severely overloaded; *(ii)* both receivers lead to a gain of 3 dB in the average SINR when the processing gain is doubled.

The results shown in this section are minor samples of the extensive efforts that have been carried out in order to validate [9] a packet network simulator that has been developed in C⁻⁻ using object oriented paradigm approach. From this point on, since the analytical results presented are

based upon some specific postulates (e.g. MRC receiver), it will be used simulation to assess the optimum 2D Rake receiver performance. Hereafter, unless otherwise stated, it is investigated the performance of optimum 2D Rake receiver overt a Rayleigh channel.

| DOA | Numerical | | Simulation | | |
|---|---|---|---|---|---|
| | Norm MAI | Mean SINR | Norm. MAI | Mean SINR | Median SINR |
| U[-10°,10°] | 4.2 | 2.9 dB | 3.8 | 3.6 dB | 3.2 dB |
| U[-20°,20°] | 2.4 | 5.2 dB | 2.5 | 5.3 dB | 5.0 dB |
| U[-30°,30°] | 1.8 | 6.6 dB | 1.8 | 6.8 dB | 6.5 dB |
| U[-60°,60°] | 1.1 | 8.7 dB | 1.1 | 9.0 dB | 8.8 dB |

**Table 1a.** Effects of DOA on the normalized MAI and SINR at receiver output with optimum response. $G_p$=64; K=40.

| | Numerical | | Simulation | | | |
|---|---|---|---|---|---|---|
| | $G_p$=32 | $G_p$=64 | $G_p$=32 | | $G_p$=64 | |
| K | MRC | MRC | MRC | Optimum | MRC | Optimum |
| 10 | 12.0 | 15.0 | 13.1 | 15.8 | 16.1 | 18.8 |
| 20 | 8.8 | 11.8 | 9.3 | 10.9 | 12.3 | 13.9 |
| 40 | 5.7 | 8.7 | 6.0 | 6.9 | 9.0 | 10.0 |

**Table 1b.** Effects of channel load on the average SINR in dB at AA coherent receiver and AA optimum receiver output. DOA is uniformly distributed between [-60°,60°]

**Table 1.** AWGN channel with perfect power control loop. M=8, $M_D$=1; SNR=100 dB. $N_{BS}$=19; f=0.6.

## 6 SOFT HANDOFF

The external interference in the target cell can be modeled as a sum of two components [5, pp. 189]:

$$I_{ext} = I_{S_0} + I_{\overline{S}_0}, \quad (30)$$

where $I_{S_0}$ denotes the component of external interference originated in the region where the MS can be controlled by the target cell. $I_{\overline{S}_0}$ is the component of external interference originated in the region $\overline{S}_0$, where $\overline{S}_0$ is the complementary region of $S_0$. Assuming an MS located at the central cell, Fig. 6 exemplifies these two regions for $N_c$=1, 2, 3, 4 and 9. Noticing that $N_c$, determined by the criterion of minimum distance, is the number of BSs qualified to assume the control of MSs located at the central cell.

In the results shown so far, it has been used a perfect instantaneous handoff, i.e. the MSs were always logically connected with the BS for which the average path loss in the downlink is minimum. It is verified that in this case $I_{\overline{S}_0} = 0$.

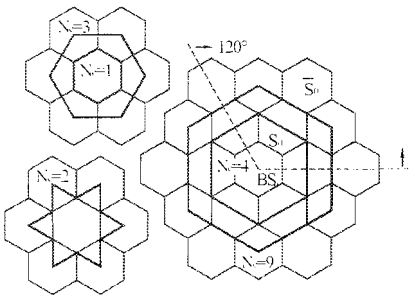


**Figure 6.** Regions $S_0$ and $\overline{S}_0$ for $N_c$=1, 2, 3, 4 e 9.

In this section it has been considered an ES Rayleigh frequency selective fading channel with 3 taps.

Fig. 7 shows the effects of number of preferential cells, $N_c$, on the throughput. The throughput is calculated as:

$$\eta = \sum_{k=0}^{K-1} k p_K(k), \quad (31)$$

where $p_K(k)$ is the probability of $k$ packets being acknowledged (ACK) at the BS when the channel is loaded with $K$ packets. The packet is ACK if the SINR at the receiver output is greater than a threshold $SINR_0$. If in Fig. 7a the path loss exponent and the standard deviation are set to 3 and 12 dB, respectively, then it is expected a considerable performance degradation when $N_c$ is not set to 19. Physically, the above characteristics occur due to the excess of the intercell interference generated in the region $\overline{S}_0$. However, if the path loss exponent and the standard deviation are set to 4 and 8 dB, respectively, then the path loss attenuates the intercell interference generates in the region $\overline{S}_0$ and thus the performance loss is not so relevant. *Mutatis mutandis*, the system performance in microcellular environments (see Fig. 7b) ratify the following important conclusion: it is necessary, even with the advanced 2D Rake receivers, a well-optimized pilot search mechanism in such way that the MSs transmit the minimum possible average power.

Hereafter, it is assumed that the "best" BS (i.e. the BS that presents the minimum medium-term attenuation) logically controls a given MS. In the following, it is fundamental to do some comparison between numerical and simulation results in order to obtain credibility to the shown simulation results.

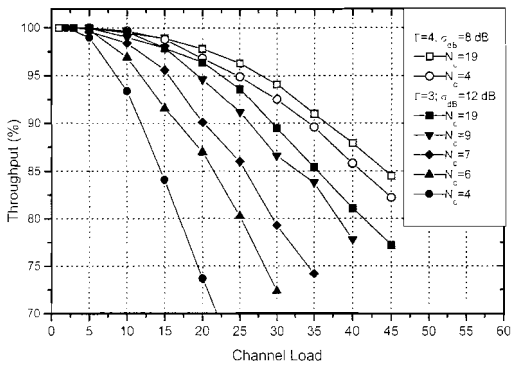


**Figure 7a.** Hexagonal macrocellular system with 19 BSs.

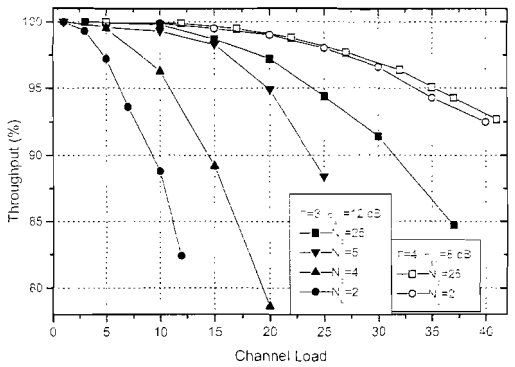


**Figure 7b.** Cross-shaped system with $X_b$=200 m.

**Figure 7.** Effects of $N_c$ on the throughput. $G_p$=64; M=8, $M_D$=1; L=P=3; SNR=10 dB; $SINR_0$=5 dB.

Using a slow PC scheme over an AWGN channel in a hexagonal macrocellular network, it is obtained the following results for the normalized mean, $f$, and for the normalized standard deviation, $\sigma_f$, of the intercellular MAI: *(i)* $f$=*0.42* and $\sigma_f$=*0.37* for $\sigma_{sh}$=*0 dB*; *(ii)* $f$=*0.6* and $\sigma_f$=*0.44* for $\sigma_{sh}$=*8 dB*; *(iii)* $f$=*0.63* and $\sigma_f$=*0.48* for $\sigma_{sh}$=*12 dB*. Comparing these results with the data plotted in Fig. 8, it is possible to observe a considerable reduction of the other-cell MAI in microcellular Manhattan environments. Fig. 8 also shows, for a hypothetical system without shadowing, a good agreement between the simulation results and the elucidative numerical results derived in [7, pp. 344-362]. Analyzing carefully these numerical results, it is verified that R. Steele, C-C Lee and P. Gould, in order to simplify a very complex scenario, did not take into account that MSs physically located in the target cell can also generate intercellular MAI in this target cell. This is absolutely true when the shadowing is absent. However, it can be noticed, in according with the two first columns of Tab. 2, discrepancies between numerical and simulation results when the lognormal shadowing is considered. Therefore, in order to validate the simulations results, it is also shown simulation results (third column of Tab. 2) where the users in the target central cell do not generate intercellular MAI (i.e. in according with the assumption used in the analytical model of [7]). These outcomes indicate the correctness of the simulation results.

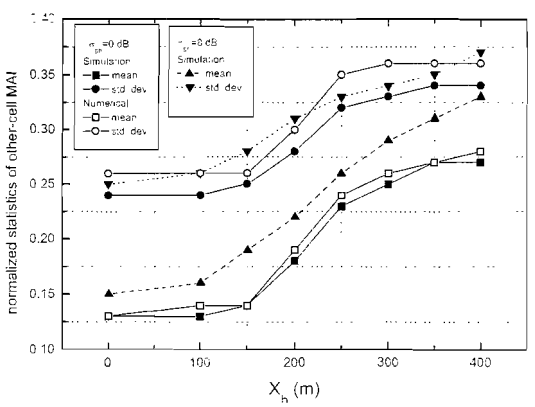


**Figure 8:** Effects of the parameter $X_b$ on the uplink normalized mean and normalized standard deviation of external interference in microcellular networks with perfect slow PC scheme over an AWGN channel.

| Γ=4 | *Simulation* | | *Numerical* | | *Simulation (see text)* | |
|---|---|---|---|---|---|---|
| $\sigma_{sh}$ | $f$ | $\sigma_f$ | $f$ | $\sigma_f$ | $f$ | $\sigma_f$ |
| *0 dB* | 0.18 | 0.28 | 0.19 | 0.30 | 0.18 | 0.28 |
| *8 dB* | 0.22 | 0.31 | 0.18 | 0.24 | 0.16 | 0.24 |
| *12 dB* | 0.26 | 0.33 | 0.20 | 0.28 | 0.18 | 0.27 |

**Table 2:** Comparison between numerical and simulation results in microcellular networks with perfect slow PC scheme over an AWGN channel. X=200 m, $X_b$=200 m.

Using the causal form of the central-limit theorem [10, pp. 234], it is possible to model the external MAI by a gamma (or chi-square) RV $I_{ext}$, whose mean and variance are obtained by multiplying the normalized values of mean and variance by the mean number of MSs loading the channel. Therefore, the covariance matrix of the received signal at target cell can be modeled as (see 8):

$$\mathbf{R} = \sum_{j=1}^{K} H_j H_j^H + \left(\sigma_n^2 + I_{ext}\right)\mathbf{I}_{MP}. \qquad (32)$$

The intercellular MAI can be also be modeled as a spatial-temporal white process characterized by its average value. Hence, (32) can be rewritten as:

$$\mathbf{R} = \sum_{j=1}^{K} H_j H_j^H + \left(\sigma_n^2 + Kf\right)\mathbf{I}_{MP}. \qquad (33)$$

where $f$ is the first moment of the intercellular MAI at the target cell.

Another possible approach is to model the covariance matrix of the received signal in a multicellular system as:

$$\mathbf{R} = \sum_{j=1}^{K} (1+f) H_j H_j^H + \sigma_n^2 \mathbf{I}_{MP}. \qquad (34)$$

It has been carried out in Fig. 9 a comparison between different approaches to model the external MAI. In Fig. 9a, it is assumed a macrocellular system with Γ=4 and $\sigma_{sh}$=8 dB, so that the normalized mean and standard deviation of external MAI are given by 0.6 and 0.45, respectively. In Fig. 9b, it is considered a microcellular system, with $X_b$=200, Γ=4, $\sigma_{sh}$=8 dB (normalized mean and standard deviation of external MAI are given by 0.22 and 0.31, respectively). 10% and 1% mean that 90% and 99% of MSs will have an SINR above the respective curve.

The simulation of full network is important to evaluate some essential aspects concerning the planning and performance assessment of cellular systems (i.e. soft and softer handoff, macrodiversity, distributed power control, and so forth). The software to simulate a full network is relatively complex. However, Fig. 9 shows that (32) to (34) allow obtaining first order results with a considerable reduction on the computational burden, since it is only necessary to simulate the target cell. Therefore, it is possible to use this approach as an important tool for software validation.

When in soft handoff, the MS is connected to $N_{soft}$ BSs, and the selection diversity is implemented on a frame basis, that is, the better frame received by either BSs is accepted by the network. To investigate the effects of soft handoff, it is assumed that: *(i)* all MSs are in soft handoff

state: *(ii)* the MSs are power controlled by the BS in which there is a lesser attenuation in the downlink.

Considering a macrocellular system, Figs. 10a, for $\Gamma$=4 and $\sigma_{dB}$=8 dB, and 10b, for $\Gamma$=3 and $\sigma_{dB}$=12 dB, show that when the channel is lightly loaded, then the soft handoff allows improvement between 1.0 and 1.5 dB in the SINR statistics observed at the 2D Rake receiver output. It can be also noticed a neglectable additional gain when more of two BSs are involved in the soft handoff. It is emphasized again that 10% means that 90% of MSs will have an SINR above the respective curve.

Supposing it is feasible to implement soft handoff with MRC technique, Fig. 11 shows that the soft handoff (actually a softer handoff) in macrocellular networks allows gains around of 2 dB in SINR observed at the 2D Rake receiver output. However, Fig. 12 indicates that in a microcellular system it is expected a reduction of the gains due to macrodiversity. Naturally, this characteristic comes upon of the greater isolation between the microcells in Manhattan networks.

In *cdmaOne* systems, for instance, the power control of MSs in soft handoff is distributed, i.e. the MS only increases its transmitted power if all BSs involved in soft handoff order to. Otherwise, the transmitted power is decreased. It can be noticed that the distributed power control reduces the intercellular MAI. In this paper it has been assumed that the MSs are power controlled by the BS with lesser attenuation in the downlink, so we can expect that the soft handoff with distributed power control allows gains still more relevant in relation to those ones showed in this section (e.g. in the link budget of *cdmaOne* systems it has been assumed a soft handoff gain of 3 dB).

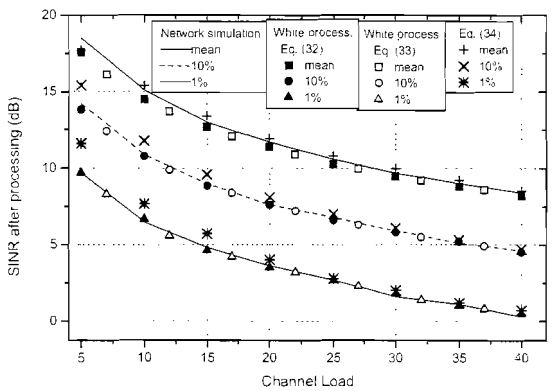


**Figure 9a.** Hexagonal macrocellular system with 19 BSs.

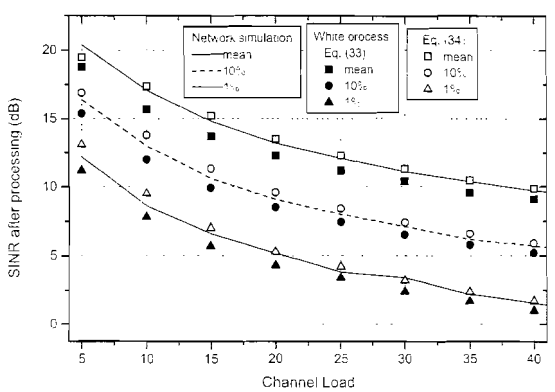


**Figure 9b.** Cross-shaped system with $X_b$=200 m.

**Figure 9.** Comparison of SINR statistics obtained with full network simulation and with intercellular MAI modeled as a white process. $\Gamma$=4 and $\sigma_{sh}$=8 dB $G_p$=64, L=P=3, M=8, $M_D$=1, SNR=10 dB.

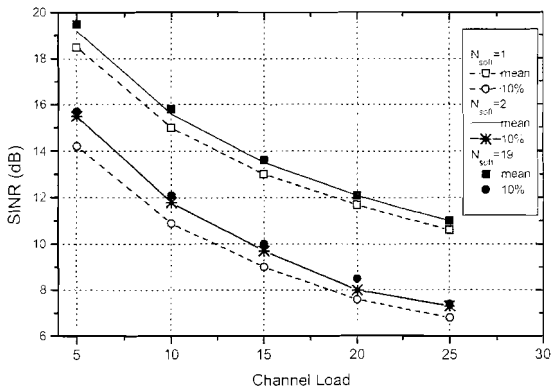


**Figure 10a.** System with 19 Bs with $\Gamma$=4 and $\sigma_{sh}$=8 dB.

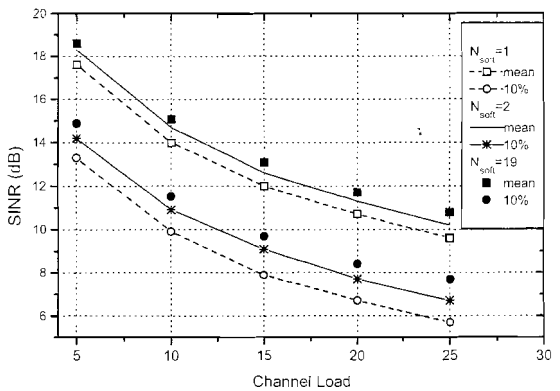


**Figure 10b.** System with 19 BSs with $\Gamma$=3 and $\sigma_{sh}$=12 dB.

**Figure 10.** Effects of soft handoff with selection diversity on the SINR statistics in a hexagonal macrocellular system. $N_{BS}$=$N_c$=19; $G_p$=64; M=8, $M_D$=1; L=P=3; SNR=10 dB.

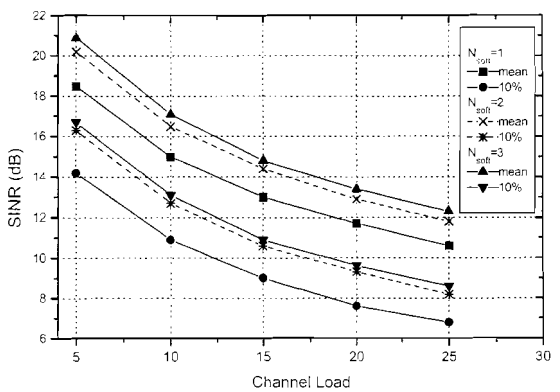


**Figure 11.** Effects of soft handoff with MRC on the SINR statistics in a macrocellular system with $N_{BS}$=$N_c$=19, $\Gamma$=4 and $\sigma_{sh}$=8 dB.$G_p$=64; M=8, $M_D$=1; L=P=3; SNR=10 dB.

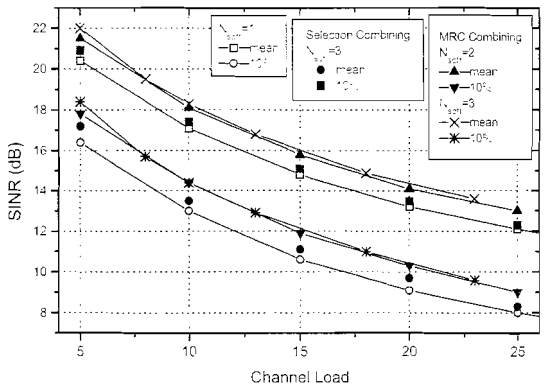


**Figure 12.** Effects of soft handoff on the SINR statistics in a microcellular system with $N_{BS}=N_c=25$, $X_b=200$m, $\Gamma=4$, $\sigma_{sh}=8$ dB. $G_p=64$; M=8, $M_D=1$; L=P=3; SNR=10 dB.

## 7 MAXMIN SINR SCHEDULING SCHEME

The dynamic allocation scheme aims at loading each time slot with MSs that have their spatial signatures with low cross-correlation and, as a consequence, it increases the SINR at the input of the detection circuit [11]. In order to accomplish an investigation on the scheduling effects on the system performance, it is assumed that: *(i)* $S$ MSs are physically located at each BS of a TDD DS-CDMA system with $N_{slots}$ time slots per uplink frame; *(ii)* each BS acquires and broadcasts information to the MSs using a MAC pooling protocol [12]; *(iii)* the channel transfer function for all MSs is known at each BS; *(iv)* the channel transfer function remains constant between the beginning of the polling period and the end of the last data uplink time slot. The MSs scheduling on the time slots is accomplished as follows: (1) the first $N_{slots}$ MSs are allocated to each slot; (2) each additional MS is assigned to the slot $n$ if the MaxMin SINR metric is fulfilled; (3) steps 2 and 3 are repeated until all MSs are assigned. In the *MaxMin* $SINR_{thr}$ metric, the step two of the previous section is done as follows: the MS being scheduled is hypothetically allocated in all time slots and the SINR is estimated for the above mentioned MS and all MSs already allocated in each time slot. The MS is definitely scheduled to the slot if the largest minimum SINR among all slots is greater than the $SINR_0$, i.e. a compatibility test is implemented.

### 7.1 SINR BOUNDS FOR ANTENNA ARRAY RECEIVERS OVER AN AWGN CHANNEL

As mentioned at Section 3, the 2D RAKE receiver reduces to an AA receiver if the number of filter taps per antenna, $P$, is set to one. For an AA receiver with perfect power control in a single-cell system, the SINR for the *k-th* user can be expressed by (see 8 and 15):

$$SINR_k = G_p \mathbf{h}_k^H \left( \sum_{j=1, j\neq k}^{K} \mathbf{h}_j \mathbf{h}_j^H + \sigma_n^2 \mathbf{I} \right)^{-1} \mathbf{h}_k , \qquad (35)$$

where $\mathbf{h}_k$ *is k-th* user's spatial signature vector. For instance, for an AA receiver with M correlated antenna the steering vector is given by (3) with the channel gain $\alpha_k$ set to one to model the perfect PC assumption.

H. Liu has derived some bounds for the MSE at the output of an AA receiver in Space Division Multiple Access Systems [2, pp. 176]. Based on these considerations, it is possible to derive some bounds for the SINR in DS-CDMA systems with AA receivers at the physical layer.

**1)** For $K \leq M$, the SINR is upper-bounded by

$$SINR \leq \frac{G_p M}{\sigma_n^2} . \qquad (36)$$

*Proof:* If the $\{\mathbf{h}_k\}_{k=1}^{K}$ spatial signatures are mutually orthogonal, then the covariance matrix of interference reduces to

$$\mathbf{R}_{U,k} = \sum_{j=1, j\neq k}^{K} \mathbf{h}_j \mathbf{h}_j^H + \sigma_n^2 \mathbf{I}_M = \sigma_n^2 \mathbf{I}_M , \qquad (37)$$

and so (36) can be directly obtained using (37) in (35).

**2)** For $K>M$, the SINR is lower-bounded by

$$SINR \geq \frac{G_p}{K - 1 + \frac{\sigma_n^2}{M}} , \qquad (38)$$

if all K user's have the same spatial signature.

*Proof:* From the matrix theory, the following inequality holds

$$\frac{M}{\lambda_1} \leq \mathbf{h}_k^H \mathbf{R}_{U_k}^{-1} \mathbf{h}_k \leq \frac{M}{\lambda_M} , \qquad (39)$$

where the ordered eigenvalues of $\mathbf{R}_{U,k}$ are $\lambda_M \leq \lambda_{M-1} \leq \cdots \leq \lambda_1$. Therefore, the maximum value of $\lambda_1$ determines the smaller lower bound of SINR. Since $tr(\mathbf{R}_{U_k}) = \sum_{m=1}^{M} \lambda_m$ is constant, then $\lambda_1$ is maximum when:

$$det(\mathbf{R}_{U_k}) = \prod_{m=1}^{M} \lambda_m \qquad (40)$$

is minimum. Using matrix properties, then (40) is minimum when all $K$ users have the same spatial signature. In this case, the determinant of $\mathbf{R}_{U,k}$ is equal to zero if the noise power is set to zero. Therefore, the covariance matrix of interference plus noise is given by

$$\mathbf{R}_{U,k} = (K-1)\mathbf{h}_k \mathbf{h}_k^H + \sigma_n^2 \mathbf{I}_M , \qquad (41)$$

and

$$SINR \geq G_p \, \mathbf{h}_k^H \left( (K-1)\, \mathbf{h}_k \mathbf{h}_k^H + \sigma_n^2 \mathbf{I}_M \right)^{-1} \mathbf{h}_k = \frac{G_p}{K - 1 + \frac{\sigma_n^2}{M}} . \qquad (42)$$

**3)** For $K> M$, the SINR is lower-bounded by

$$SINR \geq \frac{G_p}{\frac{K-1}{M} + \sigma_n^2} , \qquad (43)$$

if the following condition is satisfied:

$$\sum_{\substack{j=1 \\ j\neq k}}^{K} \mathbf{h}_j \mathbf{h}_j^H = (K-1)\mathbf{I}_M . \qquad (44)$$

*Proof:* The inequality (39) indicates that the largest lower bound of the SINR at receiver output is obtained when $\lambda_1$ is

minimum. Since $tr(\mathbf{R}_{U_k}) = \sum_{m=1}^{M} \lambda_m$ is constant, then $\lambda_1$ is minimum when

$$det(\mathbf{R}_{U_k}) = \prod_{m=1}^{M} \lambda_m \quad (45)$$

is maximum. From matrix theory, this occurs when [13]:

$$\sum_{\substack{j=1 \\ j\neq k}}^{K} \mathbf{h}_j \mathbf{h}_j^H = c\mathbf{I}_M, \quad (46)$$

i.e. when the rows of $\mathbf{h}_k \mathbf{h}_k^H$ are mutually orthogonal. It is observed that:

$$tr\left(\sum_{\substack{j=1 \\ j\neq k}}^{K} \mathbf{h}_j \mathbf{h}_j^H\right) = tr(c\mathbf{I}_M) \Rightarrow (K-1)M = cM \Rightarrow c = (K-1). \quad (47)$$

Therefore, if due to scheduling the channel is loaded with terminals whose spatial signature is fulfilled (44), then the SINR is lower bounded by:

$$SINR_k \geq G_p \frac{M}{K-1+\sigma_n^2}, \quad (48)$$

where (39) and (45) have been used in (35).

Based on Tab. 3, it can be drawn that: *(i)* the scheduling scheme significantly increases the SINR at receiver output. In these results the compatibility test is not implemented in order to make a fair comparison between analytical and the simulations results; *(ii)* the superior performance of circular array may be explained by the spatial distribution of the MSs, i.e. it is assumed that for the LES $\lambda/2$ array in a 3-sectored single cell system the DOA is uniformly distributed between $-60^0$ and $+60^0$, while for the circular $\lambda/2$ array in the one-sector single cell system the DOA is assumed to be a $U(0^0,360^0)$ RV. It is also important to emphasize the following: *(i)* the discrepancies between the theoretical and simulations results observed in a system without scheduling is expected, since this lower bound has been derived taking into account a highly improbable event (i.e. all MSs with the same spatial signature, see 41); *(ii)* although it is extremely hard for the scheduling scheme to find MSs that fits the constrain (44), the minimum SINR values obtained by simulation are relatively near to the derived theoretical lower bound (see 43).

| K | no scheduling: read (i) | | Scheduling: read (ii) | |
|---|---|---|---|---|
| | Theoretical | Simulation | Theoretical | Simulation |
| 10 | 2.5 dB | 7.3 dB<br>7.4 dB | 11.5 dB | 11.7 dB<br>12.1 dB |
| 15 | 0.6 dB | 3.7 dB<br>5.7 dB | 9.6 dB | 7.8 dB<br>9.1 dB |
| 20 | -0.75 dB | 3.0 dB<br>4.6 dB | 8.3 dB | 6.2 dB<br>7.5 dB |

**Table 3.** Theoretical SINR lower-bounds and minimum values of SINR obtained by simulation, with a maximum SINR solution, for a LES array and a circular array (second line). M=8, $M_D$=1, $G_p$=16; L=P=1; SNR=100 dB; $N_{BS}$=1.

Finally, this subsection is finished with the claim that the results shown, besides giving a mathematical insight on the interrelations between the spatial domain characteristics and scheduling schemes, also give confidence in relation to the correctness of the simulation results.

## 7.2 SYSTEM PERFORMANCE WITH AND WITHOUT SCHEDULING

Unless otherwise remarked, it is evaluated the performance of optimum 2D Rake receivers over a Rayleigh frequency selective fading channel using the default settings defined at Section 4. The number of traffic slots per uplink frame and the SNR at the receiver output are set to 10 and 10 dB, respectively.

Figures 13a and 13b show the effects of number of spatial diversity branches on the throughput when the $SINR_0$ is set to 5 dB and 8 dB, respectively. These figures show that the *MaxMin SINR* scheduling scheme allows an expressive improvement on the throughput in single-cell systems. It has also been noticed that the spatial diversity substantially improve the throughput, mainly in systems without scheduling.

Fig. 14 clearly shows that scheduling reduces considerably the variance of the SINR observed at the receiver output Ratifying the results shown in Fig. 13, it is observed that similar effects (i.e. SINR variance reduction) are obtained with spatial diversity.

Tab. 4 shows the mean and standard deviation of the SINR at the receiver output without and with scheduling (second line). When the number of users is sufficient large to avoid short-term variation of the *MAI*, then the average value of the SINR is independent of the spatial diversity.

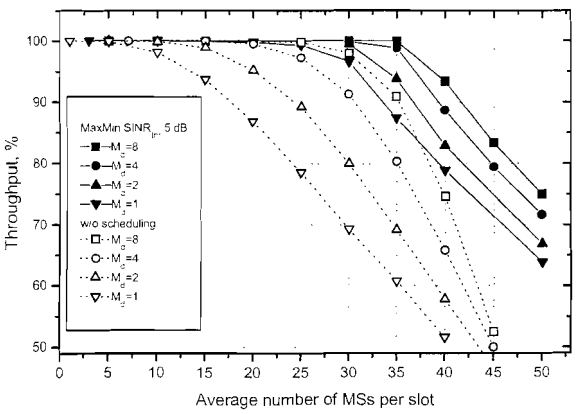


**Figure 13a.** $SINR_0$= 5 dB.

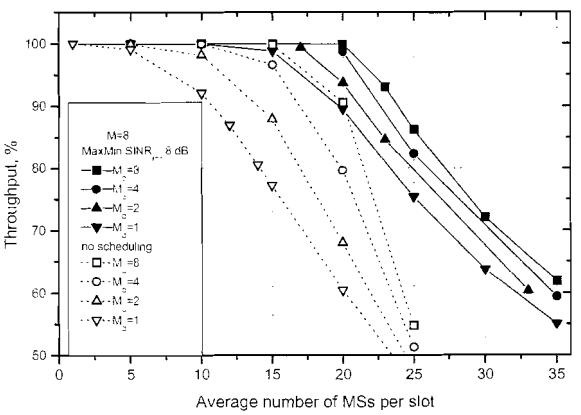


**Figure 13b:** $SINR_0$= 8 dB.

**Figure 13:** Effects of number of spatial diversity branches on the throughput in a hexagonal single cell system. $G_p$=16, M=8, L=P=3.

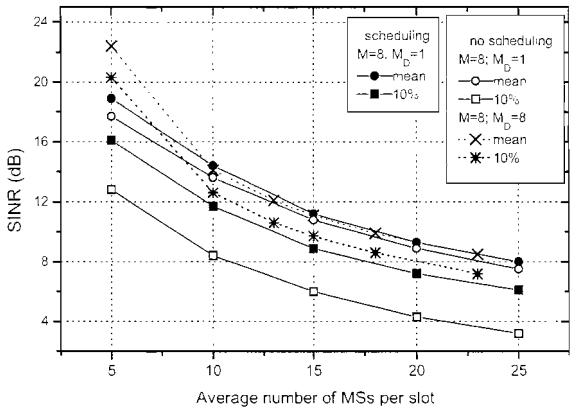


**Figure 14:** SINR statistics at 2D Rake receiver output in a hexagonal single cell system. $G_p$=16, M=8, L=P=3. $SINR_0$= 5 dB.

Fig. 15 shows a comparison between numerical and simulation results for the SINR CDF at the 2D Rake receiver output. It is assumed that a Gaussian RV in decibels, whose parameters are given in Tab. 4, can model the SINR. These results indicate that if the first moment and standard deviation of the SINR are known, then a Gaussian RV in decibels can be used as a first order estimation of the SINR at the receiver output.

| K | M=8, $M_D$=1 | | M=8, $M_D$=8 | |
|---|---|---|---|---|
| | Mean | Std. dev. | Mean | Std. dev. |
| 5 | 17.7 dB | 4.1 dB | 22.4 dB | 1.7 dB |
| | 18.9 dB | 2.7 dB | 23.5 dB | 1.4 dB |
| 10 | 13.6 dB | 4.2 dB | 14.1 dB | 1.2 dB |
| | 14.4 dB | 2.5 dB | 14.4 dB | 0.98 dB |
| 15 | 10.8 dB | 3.9 dB | 11.1 dB | 1.1 dB |
| | 11.2 dB | 2.0 dB | 11.2 dB | 0.86 dB |

**Table 4.** Mean and standard deviation of the SINR at the 2D Rake receiver output for a system without and with scheduling (second line). $N_{BS}$=1, $G_p$=16, M=8, L=P=3. $SINR_0$= 5 dB.

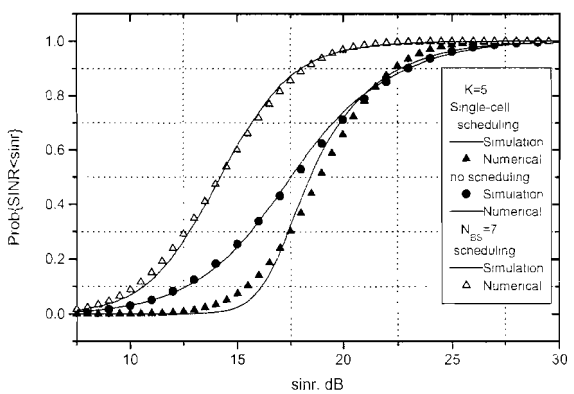


**Figure 15:** Comparison between simulation and numerical results of SINR CDF at the output of the optimum 2D Rake receiver. $G_p$=16, M=8, $M_D$=1, L=P=3; SNR=10 dB.

Taking into account that in multicellular environments the external MAI in the scheduling period is uncorrelated to the external MAI in the traffic time slots, then comparing the Fig. 16 with the Figs. 13 and 14 permits to infer that the scheduling effects on the system performance, albeit still relevant, is minor in relation to gains obtained in single cell systems. Fig. 16a also shows that when the scheduling is implemented, the improvement of soft handoff with selection combining (SC) technique on the performance is not so relevant. However, the implementation of soft-handoff with MRC technique allows considerable gains on the SINR even when the scheduling scheme is operational.

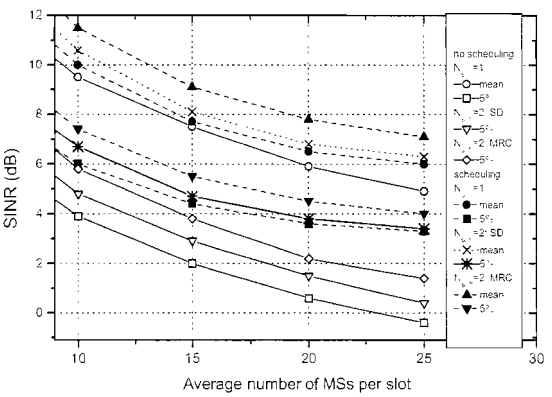


**Figure 16a**. SINR statistics. M=8, $M_D$=1. $SINR_0$= 5 dB.

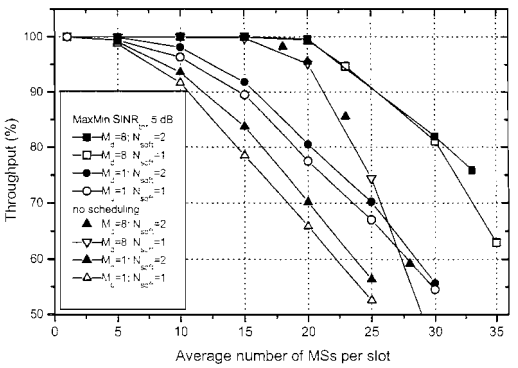


**Figure 16b**. Throughput. $SINR_0$= 5 dB; Soft-handoff with selection diversity (SD) combining.

**Figure 16.** Effects of scheduling and soft handoff on the performance of a hexagonal cellular system with 7 BSs. $G_p$=16; L=P=3.

Fig. 17 shows results for the throughput in a microcellular system considering optimum 2D Rake receiver (solid geometric figures), MRC 2D Rake receiver (open geometric figures) with scheduling (solid straight lines) and without scheduling (dash straight lines) schemes. Analysing carefully these results permit to infer that: *(i)* for an environment without diversity spatial (i.e. $M_D$=1), then the system with optimum 2D Rake receiver presents a considerable performance gain in relation to the MRC 2D Rake receiver. However, this gain performance diminishes

considerable when a system with full spatial diversity is assumed; *(ii)* the minor power unbalancing due to the full spatial diversity (i.e. $M_D$=8) reduces the gains attainable with the scheduling scheme. However, the throughput multiplication due to the scheduling is still considerable even with $M_D$=8.

Besides showing remarkable improvement due to the scheduling in microcellular cross-shaped networks, Fig. 18 shows that the parameter $X_b$ (see 27) does not influence significantly the SINR at the receiver output. Comparing Fig. 18 with Fig. 16a, it can be verified that the effects of soft handoff on the Manhattan networks are similar to those ones observed in macrocellular environments. Coherent with the results shown in Fig. 8, the outcomes of Fig. 17 indicate that the SINR does not change much when $X_b$ is increased from 1m to 200 m.

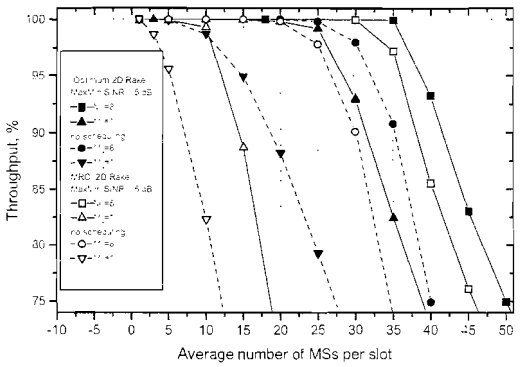


**Figure 17:** Effects of number of spatial diversity branches and of kind of 2D Rake receiver on the throughput in a microcellular single cell system. $G_p$=16, M=8, L=P=3.

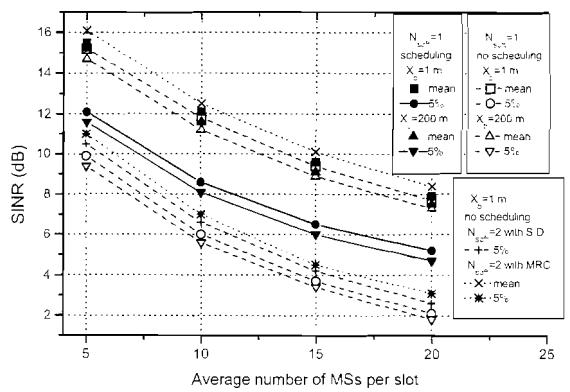


**Figure 18:** SINR statistics, parameterized by the parameter $X_b$ and $N_{soft}$, at receiver output for systems with and without scheduling in a Manhattan network. $G_p$=16, M=8, L=P=3.

Firstly, it is emphasized that when the compatibility test is operational (as in the earlier Figures of this Section), then the MSs are only scheduled if the SINR estimated at the scheduling phase is greater than a pre-established threshold $SINR_0$. For either a single-cell system without spatial diversity (Fig. 19a) and a single-cell system with full spatial diversity (Fig. 19b), it can be verified that the compatibility increases the throughput. As it has been assumed a full correlation between the channel transfer function observed in each scheduling and traffic period, then this readily explain why the throughput reaches an asymptotic platform when the compatibility test is operational. It can be verified that above a given threshold, the average number of terminals that do not pass at the compatibility test (and, therefore, they are not scheduled at each frame) increases at the same rate of channel load. However, the same phenomenon does not occur when a multicellular system is investigated (see Figs. 19c and 19d) In this case, although the compatibility test allows a considerable performance gain, this performance improvement is reduced in relation to the single-cell system since the MAI observed at scheduling period does not present a perfect correlation with the MAI effectively observed at the traffic time slots because of the intercellular interference.

Finally, the results shown in Fig. 19 indicate that there is an upper threshold where the throughput of the system without scheduling presents a better performance. It is noticed that this interesting characteristic occurs due to the high variance in the SINR statistics when the slot assignment is done in a random way. The *MaxMin SINR* scheme better equalises the SINR among the MSs in the same slot, but not for a value greater enough to overcome the $SINR_0$, when the system is overloaded.

The throughput results show in Fig. 19 (from the operator point of view) and results on the SINR statistics at receiver output show in Fig. 20 (from the user point of view) points out that the performance gain of MaxSINR receiver response in relation with the MRC receiver reduces with the spatial diversity, channel load and the intercellular MAI.

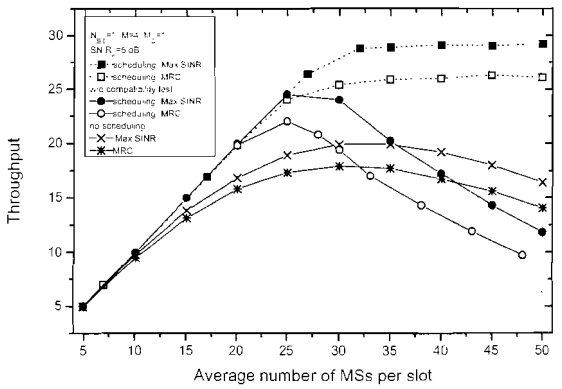


**Figure 19a.** Single-cell system with $M_D$=1.

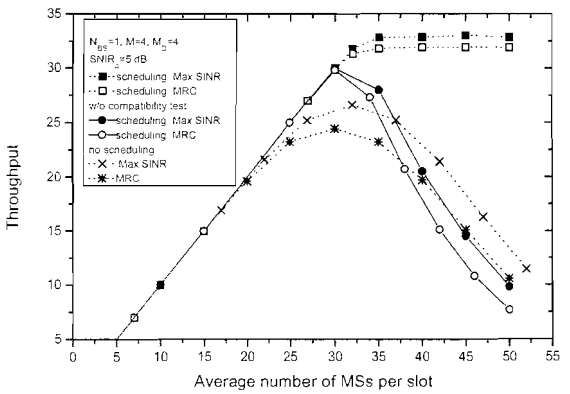


**Figure 19b.** Single-cell system with $M_D$=4.

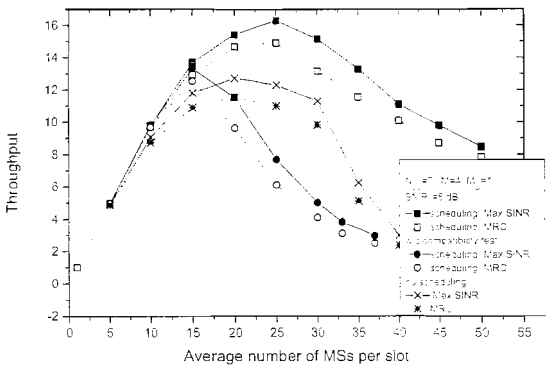


**Figure 19c.** Multicellular system ($N_{BS}$=19) with $M_D$=1.

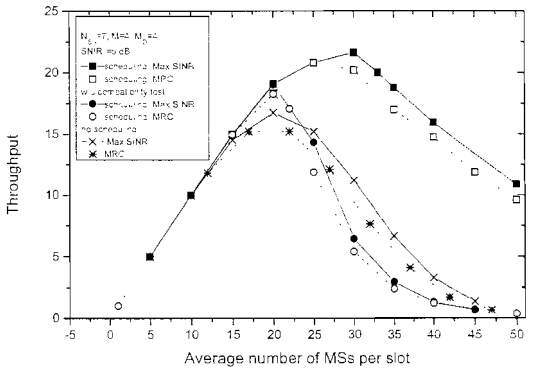


**Figure 19d.** Multicellular system ($N_{BS}$=19) with $M_D$=4.

**Figure 19.** Effects of scheduling on the throughput of a system with hexagonal cells. $G_p$=32. M=4; L=3, P=3.

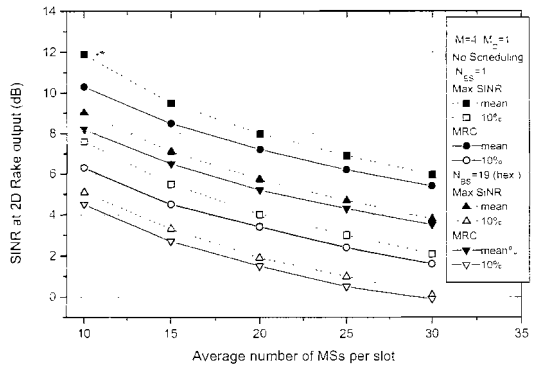


Fig **20a.** System without scheduling and without spatial diversity.

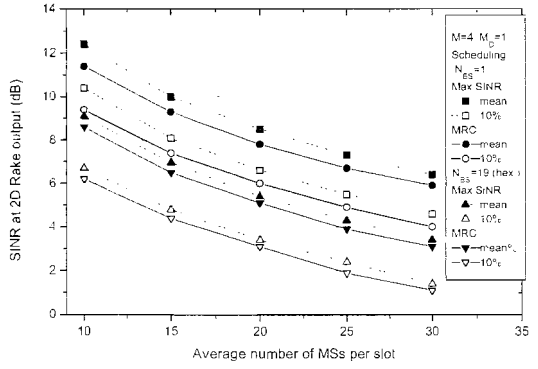


**Fig 20b.** System with scheduling and without spatial diversity.

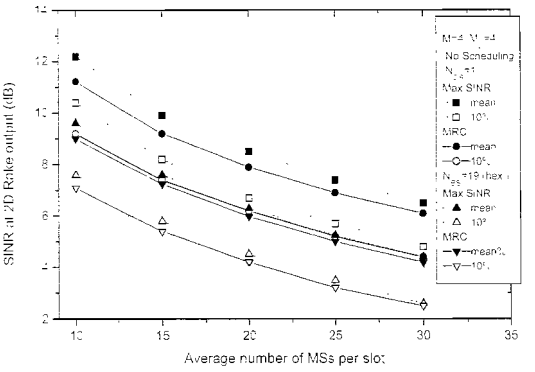


**Figure 20c.** System without scheduling and with spatial diversity.

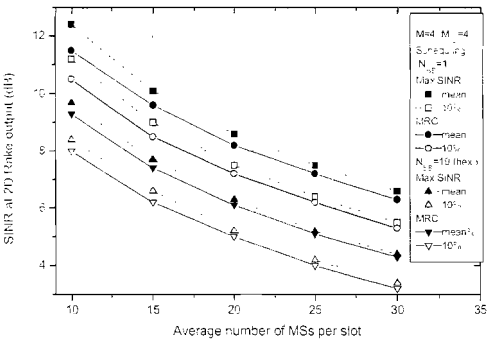


**Figure 20d:** System with scheduling and with spatial diversity.

**Figure 20:** Effects of scheduling without compatibility test as a function of channel load, spatial diversity and type of receiver (Max SINR or MRC response) on the SINR of a system with hexagonal cells. $G_p$=32. M=4; L=3, P=3.

## 8 FINAL REMARKS

Among of analytical results derived, remarks and conclusions that were done in the earlier sections, we emphasize that the dynamic time slot scheduling schemes can provide substantial improvements on the performance of TDD DS-CDMA systems with 2D Rake receivers. We also have shown that it is necessary to implement distributed power control in order to maximize the gains due to soft handoff.

Finally, it is pointed out that, *mutatis mutandis,* the dynamic time slot scheduling scheme is well suited for contention-free service with point coordination function in 802.11 and 802.11b wireless local area networks [14, pp. 140].

## ACKNOWLEDGMENT

This work is dedicated to Max Gerken (in memoriam).

## REFERENCES

[1] R. P. F. Hoefel. "On the performance of a joint TDD CDMA/PRMA and CDMA/ALOHA protocols with 2D RAKE receivers in single-cell and multi-cell networks", *IEEE VTC Fall 2001. Atlantic City, USA. 2001.*

[2] H. Liu. *"Signal processing applications in CDMA Communications"*, Artech-House, 2000.

[3] J. Litva and T. K-Y. Lo. *"Digital beamforming in wireless communication"*. Artech-House, 1996.

[4] S. Haykin. *"Adaptive Filter Theory – Third Edtion"*. Prentice Hall, 1996.
[5] A. J. Viterbi. *"CDMA: Principles of Spread Spectrum Communication"*, Addison-Wesley, 1995.
[6] R. P. F. Hoefel, C. de Almeida. "The performance of CDMA/PRMA for Nakagami-m frequency selective fading channel". *Electronics Letters*, vol. 35, no. 1, 1999, pp 28-29.
[7] R. Steele, C-C Lee. P. Gould. *"GSM, cdmaOne and 3G Systems,"* London: John Wiley & Sons, 2001.
[8] R. Prasad. *Universal wireless personal communications*, Boston: Artech House, 1998.
[9] K. Pawlikowski, H-D J. Jeong and J-S R. Lee, "On credibility of simulation results of telecommunications networks, " *IEEE Communications Magazine*, vol. 40, no. 1, pp. 132-139, 2002.
[10] A. Papoulis, *The Fourier integral and its applications*. New York: McGraw-Hill, 1962.
[11] R. P. F. Hoefel, "Dynamic time slot scheduling schemes for an uplink polling MAC TDD DS-CDMA protocol with adaptive antennas," *Electronic Letters*, vol. 38, no. 19, 2002, pp. 1131-1133.
[12] M. Zorzi. "Performance of a MAC protocol with smart antennas in a multicellular environment", *Proc. IEEE Int. Conf. Communications (ICC'2000)*, USA, 2000, pp. 402-407.
[13] B. Suard, G. Xu, H. Liu, T. Kailath. "Channel capacity of space division multiple-access schemes". *IEEE Transactions on Information Theory*, vol. 44, no. 4, July 1998.
[14] M. S Gast. *"802.11 wireless networks: the definitive guide"*, O'Relly, 2002.

**Roger Pierre Fabris Hoefel** got his Electrical Engineering degree at PUC-RS (Catholic University of Rio Grande do Sul) in 1990. In 1991 he took a *lato sensu* graduation in Electronic Instrumentation at Federal University of Santa Catarina; his Master Degree in Computer Science was taken at Microelectronic Group of Federal University of RS in 1995. In 2000, he received the Dr. degree at UNICAMP. At present he is the Telecommunication Department UNILASALLE head. His current research interests are focused on the cross layer design for high-data-rate wireless communication.

**Celso de Almeida** graduated in Electrical Engineering in 1980, got his Master and Doctor Degree at UNICAMP in 1983 and 1990, respectively. He worked in the in the telecommunication industry from 1983 to 1990. He is an Associate Professor at the Electrical Faculty of UNICAMP since 1990. His current researches are related to wireless and optical communication and cryptography.